AIP | Applied Physics Letters

Morphological effects on the field emission of ZnO nanorod arrays

Q. Zhao, H. Z. Zhang, Y. W. Zhu, S. Q. Feng, X. C. Sun et al.

Citation: Appl. Phys. Lett. **86**, 203115 (2005); doi: 10.1063/1.1931831
View online: http://dx.doi.org/10.1063/1.1931831
View Table of Contents: http://apl.aip.org/resource/1/APPLAB/v86/i20
Published by the AIP Publishing LLC.

Morphological effects on the field emission of ZnO nanorod arrays

Q. Zhao, H. Z. Zhang, Y. W. Zhu, S. Q. Feng, X. C. Sun, J. Xu, and D. P. Yu[a)]
Electron Microscopy Laboratory and State Key Laboratory for Mesoscopic Physics, School of Physics, Peking University, Beijing 100871, China

(Received 4 February 2005; accepted 6 April 2005; published online 12 May 2005)

The field-emission properties of ordered ZnO nanorod arrays with different morphologies were investigated in detail. After comparison of three different morphologies, it was found that the morphology of the ZnO nanorods has considerable effect on their field emission properties, especially the turn-on field and the emission current density. Among them, the ZnO nanoneedle arrays have the lowest turn-on field, highest current density, and the largest emission efficiency, which is ascribed to the small emitter radius on the nanoscale. On the other hand, high nanorod density remarkably reduces the local field at the emitters owing to the screening effect, which is related to the density of the emitters. The analysis results could be valuable for the application of field-emission-based devices using ZnO nanorod arrays as cathode materials. © *2005 American Institute of Physics*. [DOI: 10.1063/1.1931831]

Field emission is one of the most fascinating properties of one-dimensional (1D) nanostructured materials and has been extensively studied due to its importance both in view of fundamental science and in high-tech applications. A great deal of intensive research interests are driven by the enormous commercial applications of the vacuum electronic devices using nanostructures as cathode materials, such as field-emission flat displays,[1] x-ray sources,[2] and microwave devices.[3] Although carbon nanotubes (CNTs) have attracted much attention due to their low turn-on fields and large emission currents,[4–6] detailed study on the field-emission properties of oxide semiconductor nanowires is desirable and a lot of work has been reported. Among them, as a wide band-gap semiconductor, ZnO is a very important oxide due to its peculiar properties, such as large exciton binding energy, high thermal stability, and oxidation resistance in harsh environments. ZnO nanowires were synthesized via different methods, including the physical vapor deposition approach and using anodic alumina membranes,[7,8] and their field-emission properties have been reported, such as well-aligned ZnO nanowires grown at low temperature,[9] ZnO nanowires on a tungsten substrate,[10] ZnO nanoneedle arrays,[11,12] tetrapodlike ZnO nanostructures,[13] gallium-doped ZnO nanofiber arrays,[14] and ZnO nanowires grown on carbon cloth.[15] These works revealed excellent field-emission properties of the ZnO nanostructures and shed light on potential applications in the near future. On the other hand, in order to develop field-emission devices based on ZnO nanostructures, detailed studies are still necessary to investigate the key factors that can influence their field-emission properties. Very recently, the shape-controllable synthesis of ZnO nanorod arrays has been realized via the vapor phase growth method,[16] which provides us with a good opportunity to compare the field-emission properties of ZnO nanorod arrays with very different morphologies. In this letter, field-emission properties of three different morphologies of ZnO nanorod arrays have been investigated and compared in detail.

Three kinds of ZnO nanorod arrays with particular tip morphologies were fabricated using vapor phase growth at different conditions, and the detailed growth process and the possible growth mechanism were reported in our previous papers.[16,17] The morphologies of as-grown samples were characterized using scanning electron microscope (SEM) and the representative SEM images are shown in Fig. 1, which reveals three different morphologies of the ZnO nanorod arrays, corresponding to nanoneedle, nanocavity, and bottlelike rod arrays, respectively. These nanorods have perfect orientation perpendicular to the substrate, and are well aligned in very high coverage density. The ZnO nanoneedles have sharp tips [Fig. 1(a)], the nanocavity consists of a gradual pillar and a flat hexagonal faceted head [Fig. 1(b)], and the bottlelike nanorods consist of a well-faceted stem and a small faceted head [Fig. 1(c)]. The average radius of the nanoneedles, nanocavities, and bottlelike rods are 50, 120, and 175 nm, respectively, as summarized in Table I.

The field-emission properties of the three kinds of nanorod arrays were measured using a two-parallel-plate configuration in an ultrahigh vacuum chamber with a pressure better than 3×10^{-7} Pa at room temperature. Details of the measurement system and procedure were reported previously.[18]

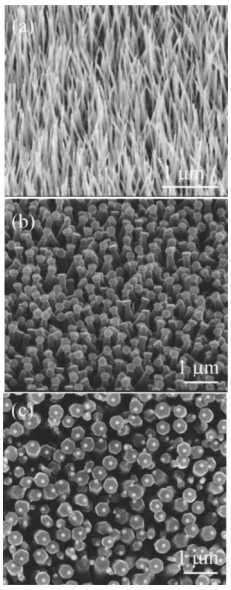

FIG. 1. Typical SEM images of the three different ZnO nanorod arrays. (a) Nanoneedles, (b) nanocavities, (c) bottle shaped.

[a)]Author to whom correspondence should be addressed; electronic mail: yudp@pku.edu.cn

TABLE I. Field emission properties and morphological characteristics of the ZnO nanorod arrays. (r: the average radius; β: the field enhancement factor obtained from the F–N plots; β_{single}: the field enhancement factor obtained from Filip model for a single emitter; Density: the nanorod density on the substrate estimated from SEM images.)

Morphology	r (nm)	Turn-on field (V/μm)	Threshold field (V/μm)	β	β_{single}	Density (/cm^2)	s	η
Nanoneedle	50	2.4	6.5	1464	9201	1.3×10^7	0.159	2.75%
Nanocavity	120	4.1	11.6	1035	3834	1.1×10^7	0.270	0.47%
Bottlelike	175	4.6	—	809	2629	5.8×10^6	0.307	0.41%

As-grown samples with different morphologies were stuck in turn onto a stainless-steel sample stage using conducting glue to act as the cathode. Another parallel stainless-steel plate served as the anode at a fixed cathode–anode spacing of 460 μm during all the measurements. A high voltage of ~5 kV was applied to the as-grown nanorod arrays before each measurement for removal of contaminants and degassing the samples. A voltage with a sweep step of ~50 V was applied between the anode and cathode to supply an electric field E to extract the electrons out of the nanorods. The emission current was monitored using a Keithley 485 picoammeter.

The field-emission results from the three samples are summarized in Fig. 2. The curves of the emission current density J vs E from the three samples are shown in Fig. 2(a). It is visible that the nanoneedle arrays has the best field-emission property with the lowest turn-on field (defined as the E where the J is distinguished from the background noise) of ~2.4 V/μm, the lowest threshold field (defined as the E where the J arrives at 1 mA/cm^2) of ~6.5 V/μm and

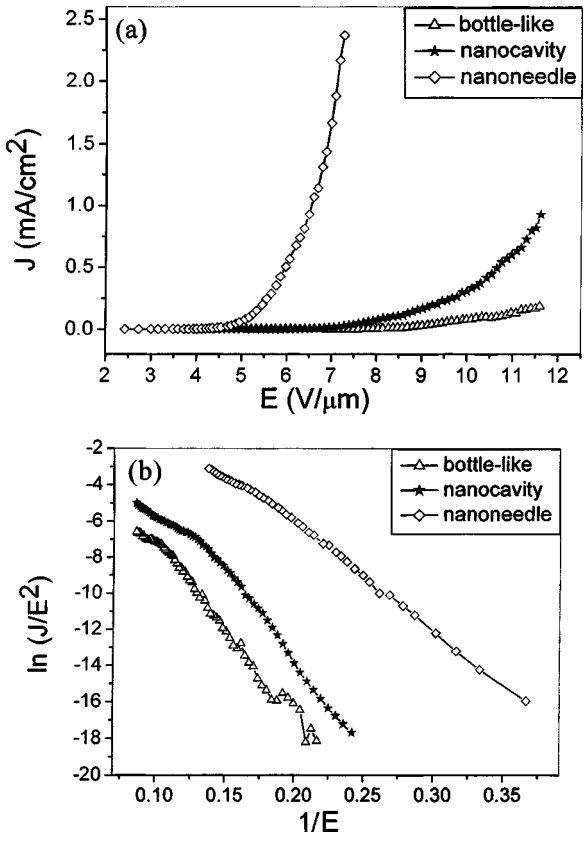

FIG. 2. (a) J–E plots of the field emission from the three ZnO nanorod arrays at a working distance of 460 μm; (b) the corresponding F–N plots showing rough linear dependence.

the highest J at the same E value. At the same time, the turn-on fields from the nanocavity and bottlelike nanorod arrays are 4.1 and 4.6 V/μm, respectively, as summarized in Table I. It is noted that the threshold field from the bottlelike structure was not be obtained due to its very small current density in the voltage range of our facility, far below 1 mA/cm^2.

To further analyze the emission properties of the above-described ZnO nanorod arrays, the classic Fowler–Nordheim (F–N) law,[19] which was induced on the base of the electron-emission properties from a semi-infinite flat metallic surface, was used to describe the relationship between the J and the local field nearby the emitter E_{local}, which is usually related to the average applied field E as follows:

$$E_{local} = \beta E = \beta \frac{V}{d}, \tag{1}$$

where d is the interelectrode spacing, V is the applied voltage and β quantifies the ability of the emitter to amplify the E and is defined as the field enhancement factor. Under this frame, the F–N law is expressed as[20]

$$J = \eta a \left(\frac{\beta^2 E^2}{\phi}\right) \exp\left(\frac{-b\phi^{3/2}}{\beta E}\right), \tag{2}$$

where $a = 1.54\times10^{-6}$ A V^{-2} eV, $b = 6.83\times10^9$ V m^{-1} eV$^{-3/2}$, and ϕ is the work function, which is estimated as 5.3 eV for ZnO.[9] The factor η describes the geometrical efficiency of electron-field emission, i.e., it is equal to the ratio of an actual emitting surface area to an overall surface area. To determine β, it is easy to trace the F–N plot through $\ln J/E^2$ vs $1/E$, which follows a linear relationship with the slope dependent of ϕ and β. The enhancement factor β can be thus determined by fitting the slope value and taking a reasonable ϕ value. Figure 2(b) corresponds to the F–N plots of the three different ZnO nanorod arrays, showing that the field-emission behaviors from the measured samples can be well described by the F–N law. In addition, the F–N plots show a straight line at low currents from every sample, and deviations were observed at a high electric field.[21] The obtained field enhancement factors from the F–N plots are also summarized in Table I. The ZnO nanoneedle has the highest β value (1464) compared to the nanocavity (1035) and bottle-like arrays (809). The β vs $1/r$ plot was given in Fig. 3 to help to find out the relationship between the β and the emitter radius. It is clear that β follows a certain trend with $1/r$, which is the smaller the radius of the emitters, the higher the β. It can be seen from Table I that the nanoneedle arrays that have the lowest turn-on and threshold fields, have the highest β and the smallest radius r. So the excellent field-emission property and the high β were closely related to the fact that the local field acted at the emitters was greatly enhanced owing to the small emitter radius on nanoscale.

On the other side, obvious nonlinearity was observed in Fig. 3, indicating that β is not exclusively determined by the emitter radius. Therefore, the Filip model was used to explain such a deviation. Considering the screening effect between adjacent emitters, E_{local} can be expressed by Filip model[22]

$$E_{\text{local}} = s\frac{V}{r} + (1-s)\frac{V}{d}, \tag{3}$$

where r is the radius of the emitter and s is a parameter describing the degree of the screening effect, which ranges from 0 for high densely arranged emitters to 1 for a single one. Combining the expression (1) with Eq. (3), another expression can be derived to estimate the field enhancement factor β from array emitters

$$\beta = 1 + s\left(\frac{d}{r} - 1\right) \cong 1 + s\frac{d}{r}. \tag{4}$$

Substituting the d value and the average r for the three different ZnO nanorod arrays as $s=1$ for a single emitter, the enhancement factors were estimated to be 9201, 3834, and 2629 for a single nanoneedle, nanocavity, and bottlelike rod, respectively, as shown in Table I. The resultant enhancement factor was defined as β_{single}, which is reasonably proportional to $1/r$. However, both the nonlinear shape in Fig. 3 and the SEM images shown in Fig. 1 indicate difference in s and nanorod density for the three samples. The emitter density can be counted statistically from the SEM images and is shown in Table I too. On the other hand, using the actual β values from field-emission measurements, the screening effect s is estimated to be 0.159, 0.270, and 0.307 for the three samples, respectively, indicating the difference in the screening effect can effectively influence the β values. Therefore, the higher the emitter density, the smaller the s, and the greater the role that the screening effect plays in the actual electron field-emission process, which in turn further decreases the β value for nanorod arrays. According to above analysis, β_{single} of the single emitter is proportional to $1/r$, but owing to the different density, leads to the different degree of the screening effects in the field-emission process, so β of the nanorod arrays was decreased in a different level and deviates from the linear dependence with $1/r$ (see Fig. 3).

Additionally, morphology not only influences the field enhancement factor β and the screening effect parameter s, but the electron emission efficiency, which is related with the factor η in Eq. (2). The ordinate intercept of the F–N plots allows one to derive the values of η. In our letter, the factor η is estimated to be 2.75%, 0.47%, 0.41% for the three different samples, as summarized in Table I. Once again, one can see that the nanoneedle arrays have the highest emission efficiency among the three samples due to their large ability to concentrate applied field. In addition, all values of the emission efficiency are rather low, which means not all nanorods involve field emission because of the selectivity of the emission site in not absolutely uniform samples.[23]

In conclusion, the field-emission properties of the three ordered ZnO nanorod arrays with different morphologies were thoroughly investigated under the frame of the F–N law and Filip model. The ZnO nanoneedle arrays have the lowest turn-on field, highest β, and largest emission efficiency owing to the smallest emitter radius on the nanoscale. On the other hand, high nanorod coverage can remarkably reduce the local field at the emitters that decrease the β owing to the screening effect. So in order to get excellent field emission, both the small emitter radius and appropriate growth coverage are necessary. The as-fabricated high ordered ZnO nanorod arrays offer a promising candidate in future device applications such as flat panel displays and high brightness electron sources.

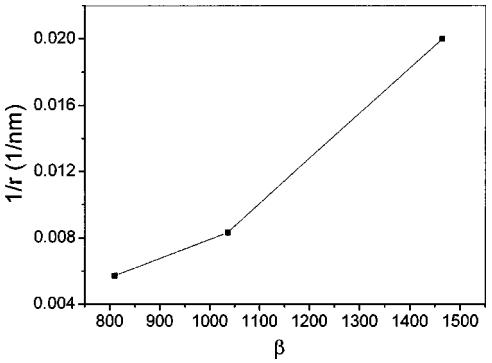

FIG. 3. β vs $1/r$ plot.

This project is financially supported by the National Natural Science Foundation of China (Grant Nos. 50025206, 50472024, 20151002), and National 973 projects (Grant No. 2002CB613505, MOST). D.P.Y. is supported by the Cheung Kong Scholar Program.

[1] R. H. Baughman, A. V. Zakhidov, and W. A. de Heer, Science **297**, 787 (2002).
[2] S. Senda, Y. Sakai, Y. Mizuta, S. Kita, and F. Okuyama, Appl. Phys. Lett. **85**, 5679 (2004).
[3] X. M. H. Huang, C. A. Zorman, M. Mehregany, and M. L. Roukes, Nature (London) **421**, 496 (2003).
[4] J.-M. Bonard, H. Kind, T. Stockli, and L.-O. Nilsson, Solid-State Electron. **45**, 893 (2001).
[5] A. M. Rao, D. Jacques, R. C. Haddon, W. Zhu, C. Bower, and S. Jin, Appl. Phys. Lett. **76**, 3813 (2000).
[6] W. Zhu, C. Bower, O. Zhou, G. Kochanski, and S. Jin, Appl. Phys. Lett. **75**, 873 (1999).
[7] Y. C. Kong, D. P. Yu, B. Zhang, W. Fang, and S. Q. Feng, Appl. Phys. Lett. **78**, 407 (2001).
[8] Y. Li, G. W. Meng, L. D. Zhang, and F. Fillipp, Appl. Phys. Lett. **76**, 2011 (2000).
[9] C. J. Lee, T. J. Lee, S. C. Lyu, Y. Zhang, H. Ruh, and H. J. Lee, Appl. Phys. Lett. **81**, 3648 (2002).
[10] L. F. Dong, J. Jiao, D. W. Tuggle, J. M. Petty, S. A. Elliff, and M. Coulter, Appl. Phys. Lett. **82**, 1096 (2003).
[11] Y. W. Zhu, H. Z. Zhang, X. C. Sun, S. Q. Feng, J. Xu, Q. Zhao, B. Xiang, R. M. Wang, and D. P. Yu, Appl. Phys. Lett. **83**, 144 (2003).
[12] H. Z. Zhang, R. M. Wang, and Y. W. Zhu, J. Appl. Phys. **96**, 624 (2004).
[13] Q. H. Li, Q. Wan, Y. J. Chen, T. H. Wang, H. B. Jia, and D. P. Yu, Appl. Phys. Lett. **85**, 636 (2004).
[14] C. X. Xu, X. W. Sun, and B. J. Chen, Appl. Phys. Lett. **84**, 1540 (2004).
[15] S. H. Jo, D. Banerjee, and Z. F. Ren, Appl. Phys. Lett. **85**, 1407 (2004).
[16] X. C. Sun, H. Z. Zhang, J. Xu, Q. Zhao, R. M. Wang, and D. P. Yu, Solid State Commun. **129**, 803 (2004).
[17] H. Z. Zhang, X. C. Sun, R. M. Wang, and D. P. Yu, J. Cryst. Growth **269**, 464 (2004).
[18] Q. Zhao, J. Xu, X. Y. Xu, Z. Wang, and D. P. Yu, Appl. Phys. Lett. **85**, 5331 (2004).
[19] R. H. Fowler and L. W. Nordheim, Proc. R. Soc. London, Ser. A **119**, 173 (1928).
[20] I. S. Altman, P. V. Pikhitsa, and M. Choic, Appl. Phys. Lett. **84**, 1126 (2004).
[21] J.-M. Bonard, K. A. Dean, B. F. Coll, and C. Klinke, Phys. Rev. Lett. **89**, 197602 (2002).
[22] V. Filip, D. Nicolaescu, M. Tanemura, and F. Okuyama, Ultramicroscopy **89**, 39 (2001).
[23] P. G. Collins and A. Zettl, Phys. Rev. B **55**, 9391 (1997).